THE AMERICAN SOCIETY OF MECHANICAL ENGINEERS
345 E. 47th St., New York, N.Y. 10017

97-GT-483

EXPERIMENTAL AND NUMERICAL INVESTIGATION OF BOUNDARY-LAYER AND WAKE DEVELOPMENT IN A TRANSONIC TURBINE CASCADE

V. Michelassi*, W. Rodi
Institut für Hydromechanik, Universität Karlsruhe
Germany

P.-A. Gieß
DLR, Institut für Strömungsmechanik, Göttingen
Germany

ABSTRACT

The flow in a transonic turbine rotor cascade is investigated by both experimental and numerical methods. Measurements include pressure profiles on the blade, total pressure profiles in the blade vane, boundary-layer and wake profiles. Computations are performed by two different solvers with different turbulence models and three different transition models. Results indicate that the introduction of transition models is necessary to have a realistic description of the flow field. Transition is shown to affect also the blade pressure distribution and shock strength mostly on the pressure side boundary layer. Experiments indicate the presence of trailiog edge vortex shedding which is not captured by the steady computations. The transition models seem adequate for predicting the shock-boundary layer interaction which induces a small flow separation on the suction side.

NOMENCLATURE

C	blade chord
k	turbulent kinetic energy
L	length scale
Re	Reynolds number
s	coordinate along blade surface
t	time
Tu	turbulence level
u	velocity
x	coordinate

greek symbols

δ	boundary layer thickness
ε	dissipation rate
λ	acceleration parameter
μ	dynamic viscosity
ν	kinematic viscosity
θ	momentum thickness
ρ	density
ω	frequency

pedices

ax	axial
cr	critical
i,j	component in the Cartesian coordinate system
in	inlet
is	isentropic
sep	at separation point
t	turbulent
tr	transitional

INTRODUCTION

The flow in modern gas turbines is often transonic involving complex phenomena such as shocks interacting with the boundary layers, and shock induced separation and transition. For the design of such turbines, reliable calculation methods are needed which must include models for simulating realistically the turbulence and transition processes and which have been validated adequately with experimental data. So far experimental and refined numerical investigations on the transitional boundary layer in transonic turbines have been rare. The present paper reports on such measurements and calculations.

In most calculations accounting for viscous effects, algebraic turbulence models have been used which do not alter the robustness and speed of the Navier-Stokes solvers. However these models often

* On leave from the University of Florence, Italy

Presented at the International Gas Turbine & Aeroengine Congress & Exhibition
Orlando, Florida — June 2–June 5, 1997

give poor accuracy (Lakshminarayana, 1991, Mayle, 1991). At the other end of the spectrum, second moment closures simulate the complex turbulence phenomena more realistically and promise more accuracy, but they require large computational effort and their superiority could not always be confirmed (Rodi et al., 1995). In the present work, the two-equation approach is adopted as a compromise between accuracy and computational efficiency. Two-equation models are generally able to yield good accuracy in terms of pressure distribution and head losses, which are of primary importance for the evaluation of the blade load and efficiency. These models will be tested here to find out how well they can describe the boundary-layer and wake behavior.

The boundary layer development is strongly influenced by transition and possible re-laminarization the modeling of which poses an additional problem. Transition can take place in several ways, which will be discussed in the following sections; it can be controlled by the local turbulence level, pressure gradient, and the flow history. Savill (1993) has given a comprehensive summary of the research in the field of by-pass transition. In his review he noted that for flat- plate boundary layers most of the two-equation formulations did not predict transition with sufficient accuracy and require an additional transition model. In turbine flows, the effect of streamline curvature and the large pressure gradients often render the tuning performed for flat plate boundary layers unreliable. Moreover, when compressibility effects play a significant role, transition may not occur via the by-pass mode but through sudden transition induced by shock-boundary layer interaction. Hence, testing for these situations is necessary.

In order to improve calculation procedures for transonic cascade flows and to allow for their adequate validation, both a computational and an experimental project were carried out in the national research program AG-TURBO of the German Ministry of Education, Science, Research and Technology. Extensive measurements in a turbine cascade flow at isentropic exit Mach number of 1.1 were carried out at DLR Göttingen, and the flow through this cascade was calculated at the University of Karlsruhe with several two-equation turbulence models, combined with various transition models. This paper reports on both experimental and computational results and compares the two.

THE EXPERIMENTAL DATA SET

Wind tunnel, cascade geometry, and blade profile

The blade contour and the cascade geometry were taken from the midspan section of a gas turbine rotor stage. A sketch of the linear cascade and some important geometrical variables are given in fig.1. Cylindrical blades were manufactured following the given profile having an accuracy of approximately 0.07% of the true chord length, C_{Bi}, at the leading edge and the trailing edge and of approximately 0.02% elsewhere.

The experiments reported in this paper were performed in the straight cascade tunnel at DLR Göttingen sketched also in fig. 1. (Heinemann, 1983). The facility is of the blowdown type with atmospheric inlet. The ambient air first enters a silica-gel dryer, subsequently passes two screens and a honeycomb flow straightened and enters the cascade after a contraction. Downstream of the cascade the flow passes an adjustable diffuser and the main butterfly valve and enters finally a large vacuum vessel. This vessel is evacuated by two sets of sliding-vane vacuum pumps. The inlet total pressure of the cascade is equal to the ambient pressure. The Reynolds number cannot

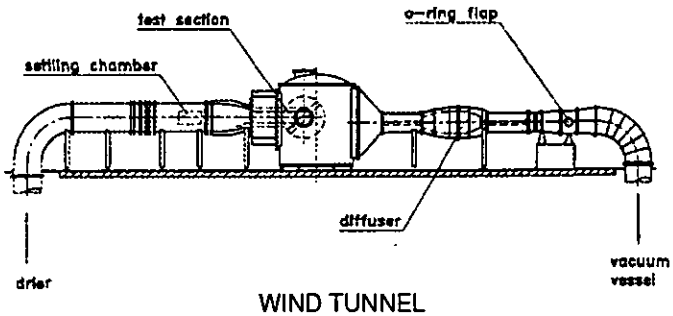

WIND TUNNEL

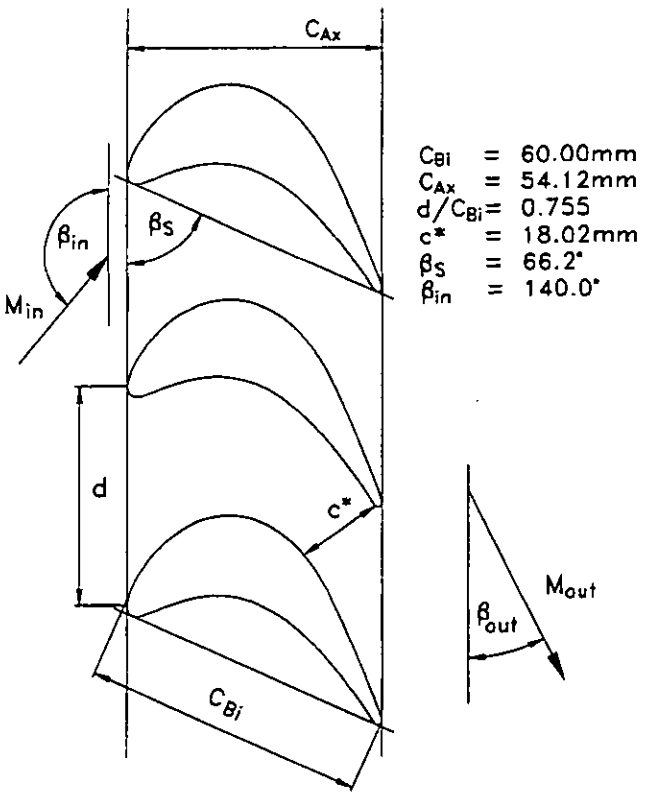

FIGURE 1. SKETCH OF THE WIND TUNNEL AND OF THE LINEAR CASCADE

be varied independently, but is a function of the Mach number. The cascade is mounted between two circular disks establishing the side walls of the flow channel. The inlet angle is adjusted by turning this assembly. The test section dimensions are 380x125mm, which allow the special cascade of these tests to consist of 15 blades, i.e. 14 blade channels with flow.

Near the center line of the tunnel the cascade support was equipped with exchangeable mineral glass panes in which six blade passages could be seen. Nevertheless only four blades were observed with the Schlieren technique and only two blade channels were accessible by the Laser two-focus velocimeter because of limited space in the plenum. The flow downstream of the cascade is not guided. The downstream static pressure and therefore the Mach number is adjusted by the plenum pressure (i.e. setting of the diffuser).

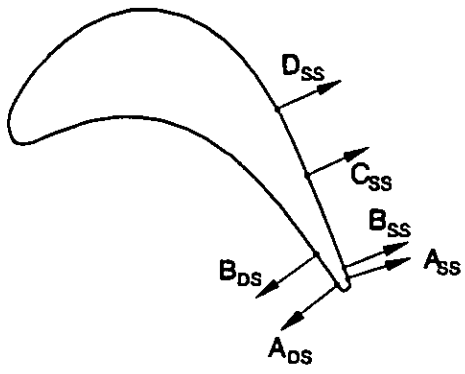

FIGURE 2. LOCATION OF THE TOTAL PRESSURE PROFILE MEASUREMENTS

Measurement technique and data reduction

In order to determine the performance of the cascade, wake flow measurements were made by traversing a wedge-type probe far behind the cascade. The calibrated probe measures total pressure, static pressure and flow angle. From the data on the inhomogeneous flow in the traverse plane, the properties of the equivalent uniform outlet flow are obtained by applying the equations of conservation of mass, momentum, and energy (Amecke, 1995). Static pressure on the blade surface was measured at midspan for two adjacent blades with 57 pressure tappings. On the rear part of the suction side and at the trailing edge the tapping density was increased to improve the spatial resolution of the flow field around the trailing edge and of the regime where the shock interacts with the suction side boundary layer and is reflected. Boundary layer measurements were made by traversing a flattened pitot-probe normal to the blade surface. Contact with the blade surface is indicated when an electric circuit, consisting of probe and blade, is closed. With the aid of the electric contact also the actual distance of the probe to the blade surface could be made zero with flow switched on. Inside the boundary layer the static pressure was assumed to be constant and was taken from previous pressure distribution measurements. In the outer part of the boundary layer supersonic velocities may occur, causing a normal shock in front of the probe. Therefore the measured value had to be corrected according to the normal shock relations. Then velocities were computed, assuming constant total temperature. From these values boundary layer displacement and momentum thickness were obtained by integration. Figure 2 shows the location of the six measured profiles.

To investigate the downstream flow field a Laser-Two-Focus velocimeter (L2F) was used, as described in detail by Schodl (1980), and Kost (1993). The measurements of the velocity components were done in axial and circumferential direction, while neglecting the radial component. The L2F-system used generates two highly focused light beams in the probe volume which act as a "light gate" for tiny particles in the flow. The scattered light provides two successive pulses with a time delay proportional to the velocity component perpendicular to the direction of the two foci and to their separation. The foci had a diameter of 8 μm and were separated by 207 μm. In order to increase the data rate, the flow was seeded by oil droplets of 0.3 μm diameter. They were produced using a special seeding generator and were injected into the flow in the settling chamber. The mean flow angle is provided by turning the second laser beam around the first one and thus accumulating velocity distributions at a certain number of angles. The whole measurement procedure was PC-controlled, automatically changing the L2F-angle, measuring the velocity distributions at the specified angles, and storing the data for each angle. The measurement position in the rotor pitch is delivered by an angular encoder. A statistical evaluation procedure gives the desired mean flow values (u, v) and the fluctuation values.

Schlieren photos were taken using a flash light of 3μs. To assure the same flow field as investigated by using the other techniques, the same pressure in the plenum has to be fixed.

Oil flow traces were taken by spraying a thin layer of a mixture of oil and vaporized titanium dioxide onto the blade surface. When the fluid passes the cascade over the blade surface, patterns develop from which photographs were taken.

MATHEMATICAL FORMULATIONS

The calculations were performed by using two well established numerical solvers. The first solver, FAST-3DC (Michelassi, 1994), is the compressible version of the pressure-correction solver developed by Zhu (1992). The method is based on the density biasing concept which allows one to use the pressure-correction equation for transonic and supersonic flows. The second solver is FLOS3D, (Michelassi and Martelli, 1993), based on an implicit time marching algorithm. Both the codes solve the mass conservation, momentum and energy equations, together with two additional transport equations for the turbulence model, which are discretized by using second order finite volumes. The turbulence models are based on the introduction of the eddy viscosity which FAST-3DC computes with a k-ε or two-layer approach, whereas FLOS3D uses the k-ω formulation. The two codes have been compared in previous investigations (Michelassi et al., 1995a, 1995b), and yielded very similar results. The differences in the predictions of transonic channel flows and a range of turbine-blade flows could be attributed to the differences in the turbulence models. For the sake of simplicity it was decided to keep the solvers unaltered so that the k-ω turbulence model was implemented in FLOS3D, whereas the two-layer models were coded in FAST-3DC.

TURBULENCE MODELS

The k-ω model

The two-equation model by Wilcox (1988) is based on the characterization of the local state of turbulence by two parameters: the turbulent kinetic energy k and the frequency $\omega=\varepsilon/k$, where ε is the rate of dissipation of k. The eddy viscosity μ_t is related to k and ε by

$$\mu_t = C_\mu \frac{\rho k}{\omega} \tag{1}$$

and the distribution of k and ω is calculated from the model transport equations:

$$\begin{cases} \dfrac{\partial \rho k}{\partial t} + \dfrac{\partial \left(\rho u_j k\right)}{\partial x_j} = \dfrac{\partial}{\partial x_j}\left[\left(\mu + \dfrac{\mu_t}{\sigma_k}\right)\dfrac{\partial k}{\partial x_j}\right] + P - \rho\omega k \\ \dfrac{\partial \rho \omega}{\partial t} + \dfrac{\partial \left(\rho u_j \omega\right)}{\partial x_j} = \dfrac{\partial}{\partial x_j}\left[\left(\mu + \dfrac{\mu_t}{\sigma_\omega}\right)\dfrac{\partial \omega}{\partial x_j}\right] + \gamma \dfrac{\omega}{C_\mu \cdot k} P - \beta\rho\left(\dfrac{\omega}{C_\mu}\right)^2 \end{cases} \tag{2}$$

in which the production rate in the case of compressible flows is:

$$P = \left\{ 2\mu_t \left[\frac{1}{2}\left(\frac{\partial u_i}{\partial x_j} + \frac{\partial u_j}{\partial x_i} \right) - \frac{1}{3}\frac{\partial u_k}{\partial x_k}\delta_{ij} \right] - \frac{2}{3}k\delta_{ij} \right\} \frac{\partial u_i}{\partial x_j} \qquad (3)$$

The model constants are those specified by Wilcox in the original version of the k-ω model: β=3/40, C_μ=0.09, γ=5/9, σ_ω=σ_k=2. On solid walls k is set to zero and ω is computed following Wilcox (1988) for smooth walls.

The k-ω model was found to overestimate the turbulent kinetic energy in stagnation points (i.e. near the leading edge of turbine blades). This is due to the overproduction of turbulence which is controlled by equation (3).

As shown by Kato and Launder (1993), the overprediction of k is caused by the form of the production term in equation (3). To avoid this, they reformulated P as the product of rotational Ω and irrotational S contributions:

$$P = \mu_t \cdot \left[S \cdot \Omega - \frac{2}{3} D \cdot D \right] \qquad (4)$$

in which:

$$S = \sqrt{\frac{1}{2}\left(\frac{\partial u_i}{\partial x_j} + \frac{\partial u_j}{\partial x_i} \right)^2}, \quad \Omega = \sqrt{\frac{1}{2}\left(\frac{\partial u_i}{\partial x_j} - \frac{\partial u_j}{\partial x_i} \right)^2}, \quad D = \left(\frac{\partial u_j}{\partial x_j} \cdot \delta_{ij} \right)$$

The D term accounts for the not divergent-free nature of the compressible flow. The Kato-Launder modification leads to a reduction of the turbulence production rate in stagnation regions. It is entirely ad hoc, but improved significantly the predictions in various turbine-blades and was hence employed here in the k-ω model.

The two-layer model TLK

The two-layer model retains the standard high-Re version of the k-ε model outside of the viscous sublayer near solid boundaries. This model characterizes the turbulence by two parameters k and ε, which are determined from the following equations:

$$\begin{cases} \dfrac{\partial \rho k}{\partial t} + \dfrac{\partial (\rho u_j k)}{\partial x_j} = \dfrac{\partial}{\partial x_j}\left[\left(\mu + \dfrac{\mu_t}{\sigma_k} \right) \dfrac{\partial k}{\partial x_j} \right] + P - \rho\varepsilon \\ \dfrac{\partial \rho \varepsilon}{\partial t} + \dfrac{\partial (\rho u_j \varepsilon)}{\partial x_j} = \dfrac{\partial}{\partial x_j}\left[\left(\mu + \dfrac{\mu_t}{\sigma_\varepsilon} \right) \dfrac{\partial \varepsilon}{\partial x_j} \right] + c_1 \dfrac{k}{\varepsilon} P - c_2 \rho \dfrac{\varepsilon^2}{k} \end{cases} \qquad (5)$$

The turbulent viscosity is computed as:

$$\mu_t = c_\mu \rho \frac{k^2}{\varepsilon} \qquad (6)$$

The model constants are the standard high-Re values: c_μ=0.09, c_1=1.44, c_2=1.92, σ_ε=1.3, σ_k=1.

In the viscous sublayer near the wall, a one-equation model is used in which the length scale is prescribed empirically and the ε-equation is not solved. Two versions were tested (Michelassi, 1996), namely the Norris and Reynolds (1975) model using $\sqrt{k}$ as velocity scale, and the model by Rodi et al., (1993), using the normal fluctuations $\sqrt{\overline{v^2}}$ as velocity scale. Both formulations gave almost identical results for the present test case so that only the former is included here. In the Norris-Reynolds model, the eddy viscosity is computed from:

$$\mu_t = c_\mu \cdot f_\mu \cdot L \cdot \sqrt{k} \cdot \rho \qquad (7)$$

and the dissipation rate ε in the k-equation by:

$$\varepsilon = \frac{k^{1.5}}{L}\left(1 + \mu \frac{12.98}{\sqrt{k}\, L\rho} \right) \qquad (8)$$

The distribution of the length scale L is prescribed by

$$\left.\begin{aligned} L_1 &= C_D \cdot \min\left(K \cdot y, 0.085 \cdot \delta \right) \\ L_2 &= C_D \cdot \min\left(K \cdot y, \left. \frac{k^{3/2}}{\varepsilon \cdot C_D} \right|_e \right) \end{aligned}\right\} \Rightarrow L = \max\left(L_1, L_2 \right) \qquad (9)$$

in which the subscript 'e' indicates a quantity evaluated at the edge of the boundary layer, and 'y' is the distance from the wall.

The damping function f_μ in equation (7) is introduced to ensure that $\mu_t \propto \left(y^+ \right)^3$ very close to the wall. It reads

$$f_\mu = 1 - e^{-\left(0.0198 \cdot R_y \right)}$$

where $R_y = \frac{\rho \cdot y \cdot \sqrt{k}}{\mu}$ is the turbulent Reynolds number based on the wall distance. The model coostants are K=0.41, C_d=6.085. The two models for the oear-wall and outer region are matched where $f_\mu \approx 0.9$, which is equivalent to $\frac{\mu_t}{\mu} \approx 36$ in boundary layers.

On solid walls, the turbulent kinetic energy is set to zero, while the dissipation rate assumes a finite value which can be computed by equation (8).

TRANSITION MODELS

Transition to turbulence and relaminarization may both occur in turbine flows and is strongly influenced by the large pressure gradients, positive and/or negative. Since natural transition is very unlikely to take place on turbine blades, transition is normally of the by-pass type or caused by a flow separation or a shock (Mayle, 1991). In the first case transition is induced by the disturbances to the boundary layer produced by the free-stream turbulence, whereas in the second case it is a shock or a local flow separation which starts the transition process.

Although real turbine stages operate under large turbulence levels which are mainly responsible for by-pass transition, at high Mach number flows the presence of shocks, if accompanied by low turbulence levels, can be the main source of transition, as expected in this experimental cascade eovironment. In transonic turbine blades the

trailing-edge shock departing from the pressure side impinges on the suction side of the neighboring blade, thereby interacting with the boundary layer. When the boundary layer is turbulent, the impinging shock thickens the boundary layer causing increased total pressure losses. If the boundary layer is laminar, the flow can separate and transition takes place in the separated shear layer or near the reattachment point.

Transition models applied to transonic turbine flows normally evaluate a critical Reynolds number which, if exceeded, indicates that transition has started. One of the most common approaches for the computation of the critical Reynolds number is the use of the empirical formulation proposed by Abu-Ghannam and Shaw (1980). The length of transition can be modeled by a number of methods which are all aimed to give a smooth transition from the laminar to the turbulent state of the boundary layer.

The models included in this investigation are those proposed by Cho et. al. (1993), Michelassi (1996), and by Rodi, and Schönung(1987), which will be described in the next sections. These models require the computation of integral boundary layer parameters which necessitate an estimate of the boundary layer thickness δ. This is not a trivial task in turbine flows because of the highly distorted velocity profiles which prevent the use of the definition of δ as the wall distance where the velocity is 99% of the potential velocity on both the suction and pressure sides. After intense numerical testing (Michelassi, 1996), it was decided to define the boundary layer edge as the point at which:

$$\varpi = \varpi_{min} + (\varpi_{max} - \varpi_{min}) \cdot 0.01$$

in which ϖ_{min} and ϖ_{max} are respectively the minimum and maximum values of the vorticity ϖ in the cross section. This definition ensures smooth and well behaved shapes of the boundary layer thickness and a reliable method to compute the velocity at the edge of the boundary layer.

The transition model for TLK

The two-layer model TLK is particularly suited for the introduction of a transition model because of the structure adopted for the damping function f_μ. This is modified as follows, by including the ratio $25/A^+$ which acts as an intermittency function (Cho et. al., 1993):

$$f_\mu = 1 - e^{-\left(0.0198 \cdot R_y \cdot \frac{25}{A^+}\right)} \tag{10}$$

The parameter A^+ is given a large value (300) in laminar flows to make the turbulent viscosity μ_t very small and the usual value of A^+ =25 for fully turbulent boundary layers. In the transition region A^+ is calculated from:

$$A^+ = A_t^+ + \left(300 - A_t^+\right)\left[1 - \sin\frac{\pi}{2}\left(\frac{Re_\theta - Re_{tr}}{Re_{tr}}\right)\right]^2 \tag{11}$$

The dependence of A_t^+ nn the pressure gradient is neglected by imposing $A_t^+ = 25$. In transitional boundary layers A^+ gradually decreases to reach the asymptotic value of 25, characteristic of fully turbulent boundary layers.

Transition starts when the momentum thickness Reynolds number Re_θ exceeds a critical Reynolds number Re_{tr}, and it is completed when $Re_\theta = 2 \cdot Re_{tr}$. The critical Reynolds number is calculated from the following empirical relation of Abu-Ghannam and Shaw (1980):

$$Re_{tr} = 163 + \exp\left[F(\lambda) - \frac{F(\lambda) \cdot Tu}{6.91}\right] \tag{12}$$

in which Tu is the free stream turbulence level determined at the edge of the boundary layer, and

$$F(\lambda) = \begin{cases} 6.91 + 12.75 \cdot \lambda + 63.64 \cdot \lambda^2 & \text{if } \lambda \le 0 \\ 6.91 + 2.48 \cdot \lambda - 12.27 \cdot \lambda^2 & \text{if } \lambda > 0 \end{cases} \tag{13}$$

λ is the Pohlhausen acceleration parameter defined as:

$$\lambda = -\frac{\theta^2 \cdot \frac{\partial p}{\partial x}}{\mu \cdot U_{be}} \tag{14}$$

in which θ is the momentum thickness. The pressure gradient and the velocity U_{be} parallel to the solid wall are computed at the edge of the boundary layer.

The original correlation was proposed for the range $-0.1 \le \lambda \le 0.1$, but in turbine flows λ is often larger than this limit. Although the correlation could be used outside its tuning range, it was decided not to extrapolate the validity of equation (14) outside the range used in its development, and to limit the absolute value of the acceleration parameter λ in equation (13) to 0.1.

The transition model is implemented in the boundary layer only. Outside the boundary layer the flow is assumed turbulent and the damping function given by equation (13) is set to unity.

The transition model for k-ω

The absence of any damping function in the k-ω model requires the introduction of an intermittency function f_t in equation (1) which is accordingly mndified to:

$$\mu_t = f_t \cdot C_\mu \cdot \frac{\rho k}{\omega} \tag{15}$$

The onset of transition is determined by using the Abu-Ghannam and Shaw (1980) correlation, and transition is completed when $Re_\theta = 2 \cdot Re_{tr}$, as introduced for the TLK model. The function f_t is computed by rewriting equatinn (11) in the form of an intermittency function as follows:

$$f_t = \left(\frac{A_t^+}{A_t^+ + (300 - A_t^+)\left(1 - \sin\frac{\pi}{2}\left(\frac{Re_\theta - Re_{tr}}{Re_{tr}}\right)\right)}\right)^\alpha \tag{16}$$

in which α was set equal to 2. The intermittency function (16) is valid inside the boundary layer only, whereas f_t is set to unity outside the

boundary layer. The parameter α in equation (16) controls the slope of the rise of f_t in the transition region. When α is set to unity, equation (16) gives a smooth transition, whereas the transition length is somewhat increased when α=2-3 because of the decreased turbulent viscosity and growth of the boundary layer.

The transition model for separated flow

The previous transition models are not suitable in presence of laminar separation bubbles, induced e.g. by a shock. Rodi and Schönung (1987) retuned the model proposed by Kwon and Pletcher (1982) for the prediction of subsonic separation bubbles on airfoils and subsonic turbine blades where the low inlet turbulence level prevented the by-pass transition in favour of the separated flow transition. The viscous-inviscid interaction code used for the computations by Rodi and Schönung proved adequate for transitional shockfree flows. This model was also successfully implemented for the computation of transitional flows in presence of laminar separation bubbles by Papanicolaou (1996) and by Michelassi (1996) for transonic turbine blades.

In the Rodi and Schönung model transition can occur only in presence of a flow separation. As soon as a separation point is detected, transition is started when the local Reynolds number based on the momentum thickness, Re_θ, exceeds the critical Reynolds number given by:

$$Re_{tr} = \sqrt{\left(1+\frac{0.05}{\exp(0.365\cdot Tu)}\right)\cdot Re_{\theta,sep}^2+\frac{17000}{\exp(0.509\cdot Tu)}} \qquad (17)$$

in which $Re_{\theta,sep}$ is the Reynolds number based on the momentum thickness θ at the separation point. The intermittency function is computed starting from the transition point as follows:

$$f_1 = 1-\exp\left[-G\cdot(x-x_{tr})\int_{x_{tr}}^{x}\frac{dx}{U_e}\right] \qquad (18)$$

in which:

$$G = \frac{\exp(0.99\cdot Tu)}{100}\cdot\frac{U_e^3}{\nu^2}\left(Re_{\theta,tr}\right)^{-8/3} \qquad 19)$$

and U_e is the velocity at the boundary layer edge. The coordinates x and x_{sep} are defined along the blade surface. The intermittency function tends to unity gradually as the distance of the current cross section from the point of the onset of transition ($x-x_{tr}$) increases. The effect of the turbulence level is accounted for in equation (19), whereas the integral in equation (18) considers the local acceleration.

The separation bubble transition model was successfully introduced in the k-ω turbulence model only. In fact the calculations with the two-layer model showed no flow separation on the suction side so that the transition model for separated flows was never switched on.

The intermittency function is introduced according to equation (18). When using this transition model the pressure side was assumed laminar due to the absence of any recirculation bubble on this side of the blade.

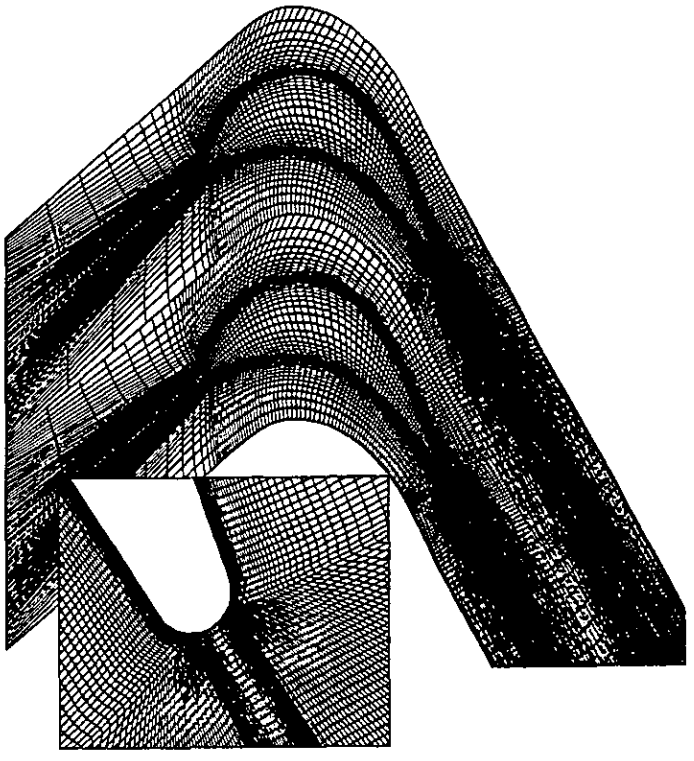

FIGURE 3. I-TYPE GRID

RESULTS AND DISCUSSION

Figure 1 sketches the cascade and specifies the geometrical parameters. The isentropic exit Mach number is 1.1 and the Reynolds number based on the exit velocity and on the chord is approximately 1.4×10^6. The inlet flow angle is 140-deg. The measured inlet turbulence level is 0.6%, and the inlet turbulence length scale L was set to 1% of the pitch. Accordingly the inlet dissipation rate ε in the TLK model and the inlet frequency ω in the k-ω model were computed as:

$$\varepsilon_{in} = \frac{\sqrt{k^3}}{L} \qquad \omega_{in} = \frac{\sqrt{k}}{L}$$

Although the turbulence level in real turbine blades is normally quite high (up to 5-10%), low turbulence level flows allow the separated flow transition to be studied in case of shock-boundary layer interaction.

Measurements include pressure distribution around the blade and boundary layer and wake profiles, part of which are given in Gieß (1994), Kost, (1994).

A set of preliminary runs determined the mesh requirements for obtaining grid independent results. The final grid adopted for the calculations has 309×151 points (approximately 40.000 points), which allowed the first grid point away from the wall to be placed at $y^+\approx$2-3. Figure 3 shows every other point of the final I-grid, in which the blade is embedded in the computational domain, and a blow-up of the trailing edge region. The periodic boundaries do not have a point-to-point periodic distribution which guarantees a weak grid skewness in

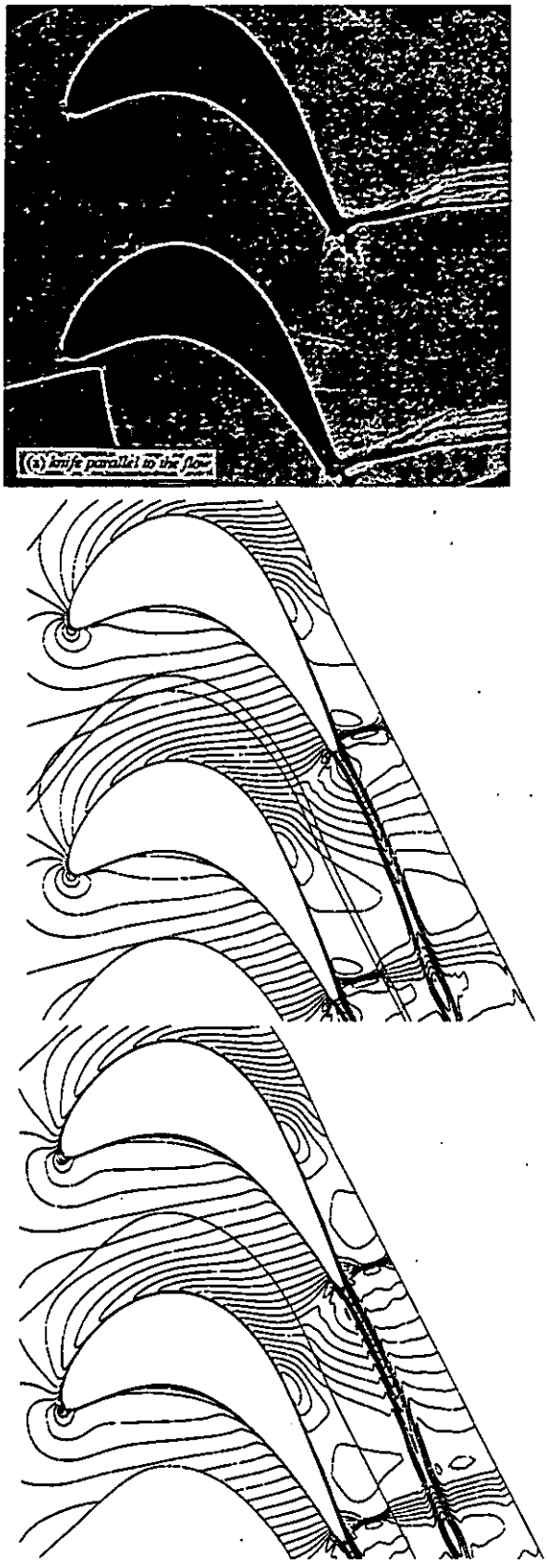

FIGURE 4.a) EXPERIMENTAL SCHLIEREN PHOTO-b) TLK MACH NUMBER ISOLINES-c) k-ω MACH NUMBER ISOLINES

the wake, but also require the interpolation of the transported quantities along all these boundaries.

FLOS3D required approximately 1500 iterations to converge, whereas more than twice as many iterations were needed by FAST-3DC to reach the same residual level of approximately 10^{-6}. Further computational details may be found in Michelassi (1996).

The experimental and computed overall flow fields are compared in figures 4,a,b,c. In figure 4,a the Schlieren flow visualization shows a strong shock departing from the suction side somewhat upstream of the trailing edge, which widens when crossing the wake of the neighboring blade. On the pressure side of the trailing edge, the shock is much weaker and hard to detect in the photograph. This shock impinges on the suction side of the neighboring blade where it is reflected. The Schlieren photo does not show any boundary layer thickening after the shock impingement on the suction side. Figures 4,b,c show the local Mach number contours computed by the transitional TLK and k-ω models respectively. The agreement is quite good in terms of shock location and inclination for both the models. The widening of the computed shock wave across the periodic boundaries is due to the sudden change in grid spacing implied by the non point-to-point periodic grids (Michelassi, 1996). Observe that the branch of the trailing edge shock which departs from the suction side starts somewhat upstream of the trailing edge. In inviscid calculations (Michelassi, 1996) the shock departs right at the trailing edge. This indicates that the upstream shift of the shock is due to viscous effects and is probably connected to the boundary layer growth caused by the shock-boundary layer interaction.

Figures 5,a,b compare the measured isentropic Mach number distribution around the blade with various k-ε model predictions. The plots include the results obtained by using the standard wall function approach and the two-layer model without transition model (TLK). These two results do not differ much. In these two calculations the Mach number drops too fast after x/Cax=0.9 (see figure 5,b) thereby indicating a strong pressure recovery absent in the experiments. When using the transition model (TLK trans.) the agreement improves in the critical region immediately upstream of the trailing edge on the suction side since the isentropic Mach number does not drop as before and it closely resembles the measurements. Figures 6,a,b show the results obtained by using the transitional k-ω model. The figure includes the results computed by the attached-flow transition model assuming either a laminar or a transitional flow on the pressure side, and the separated-flow model (s-transition). The fully turbulent calculations (not shown) led to the same problem discussed for the k-ε model calculations (Michelassi, 1996). Although the agreement is generally good (figure 6a), figure 6b shows that the assumption of laminar flow on the pressure side, which seems justified by the strong acceleration, yields an underestimation of the isentropic Mach number for x/Cax>0.85 and an overestimation of the shock strength. Apparently the strength of the expansion wave and the shock which departs from the pressure-side and impinges on the suction-side is controlled by the nature of the pressure side boundary layer. The plots indicate that the correct shape on M_{is} across the transonic region on the suction side is obtained only when a transition model is used on the pressure side. The plots show that the blade load, which can be computed by the pressure distribution around the blade, is influenced by the transitional nature of the boundary layer

Figure 7 shows the oil flow visualization on the suction side (Bräunling et al., 1988). In proximity to the side walls, the passage vortex grows when approaching the trailing edge, but the mid-span

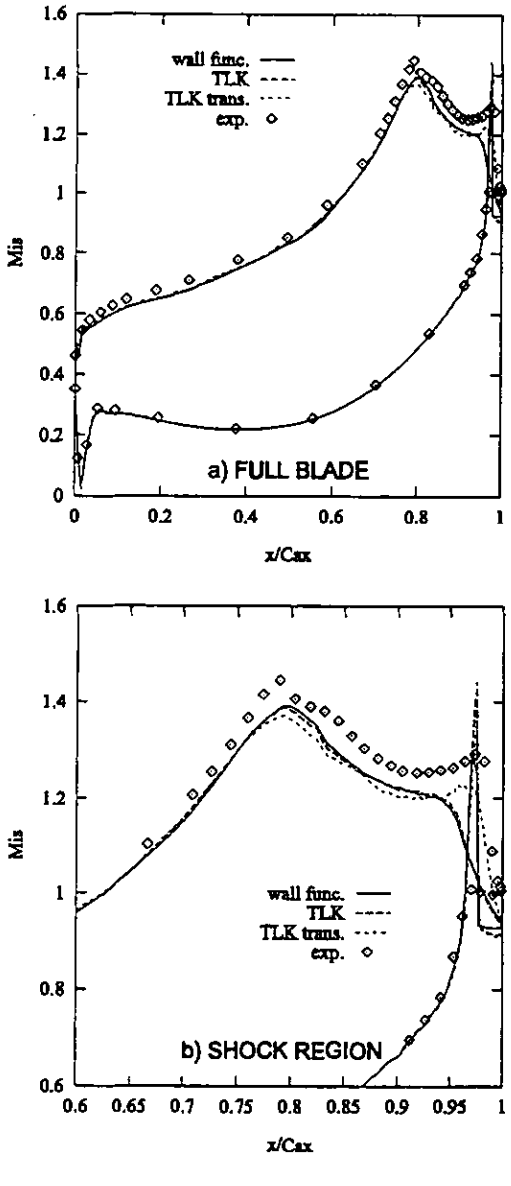

FIGURE 5. ISENTROPIC MACH NUMBER, K-ε MODEL.

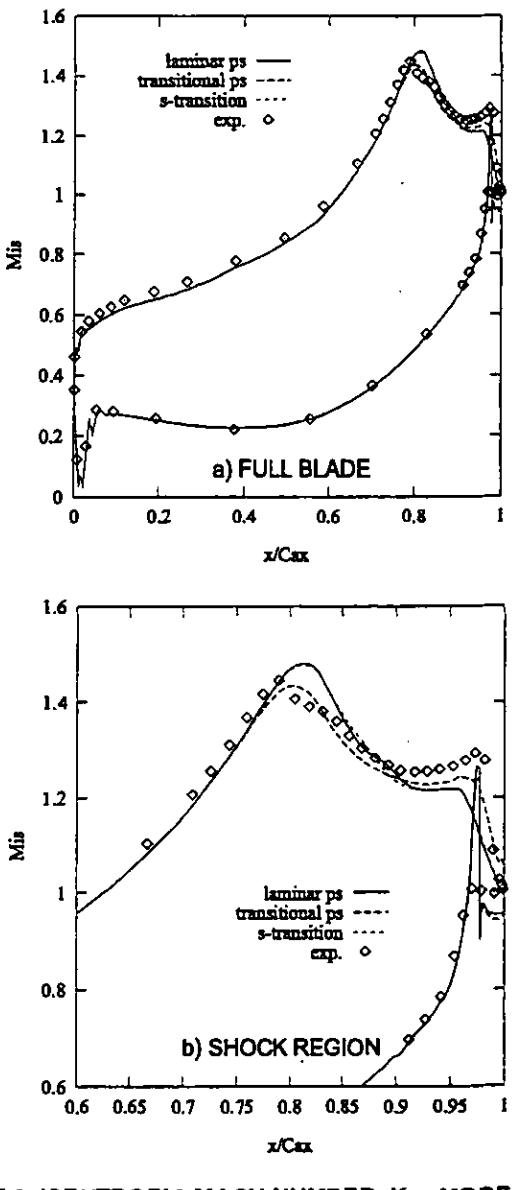

FIGURE 6. ISENTROPIC MACH NUMBER, K-ω MODEL

section of the blade does not seem to be affected and there the flow can be considered two-dimensional, as confirmed by the value of the stream tube contraction ratio which is approximately 0.962.

. The figure also shows a small flow separation where the shock impinges on the suction side, the size of which is difficult to estimate from the picture. The transitional two-layer model was unable to predict this small flow separation so that the separated flow transition model could not be used in the TLK formulation. The k-ω model was able to detect the small separation bubble, which starts when the boundary layer is still laminar, only when assuming a transitional boundary layer on the pressure side. The same bubble was also detected when using the separated flow transition model which assumes a laminar pressure side.

Figures 8a compares the computed (by using transition models) and measured boundary layer thickness δ on the suction side. There, the experiments indicate that the boundary layer stays laminar up to the shock because of the very low inlet turbulence intensity. The measurements indicate also a steep rise in δ after the shock (Gieβ,1994). The shock-boundary layer interaction seems to be reproduced better by the TLK model which reproduces this rise with good accuracy on the suction side.

Figure 8b compares the measured and computed boundary-layer thickness δ on the pressure side. The thickness δ can be seen to increase in the first part of the blade. Then the flow encounters a strong favorable pressure gradient and accelerates, thereby reducing the thickness of the boundary layer. The k-ω model predicts the right boundary-layer thickness close to the trailing edge, whereas the TLK model slightly underestimates it. The measurements indicate that the boundary layer on the pressure side is laminar up to the location of the velocity peak and then becomes turbulent despite the effect of the

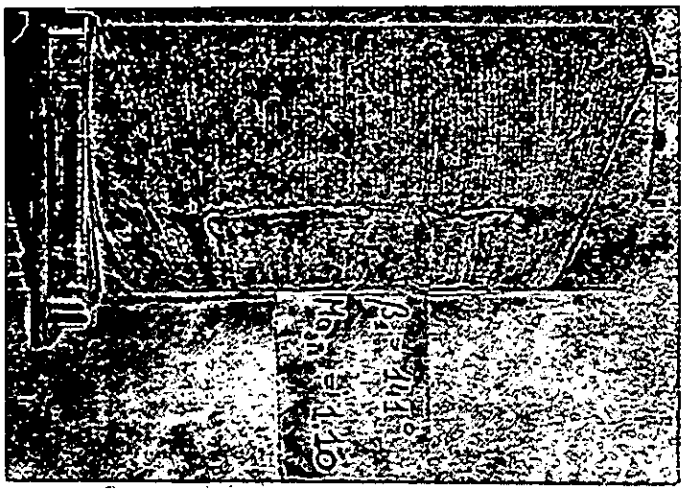

FIGURE 7. OIL FLOW VISUALIZATION ON SUCTION SIDE

strong flow acceleration towards the end of the blade. In figure 9b the computations are shown to predict transition somewhat downstream at approximately x/Cax=0.15. Then both the predicted f_t functions decrease thereby indicating a sort of relaminarization of the boundary layer, although in the k-ω model the intermittency function does not reach the lower laminar limit. Nevertheless this phenomenon has a small effect on the boundary-layer calculation since it is mainly the flow acceleration which considerably reduces the thickness δ.

Figure 8c compares the predicted momentum thickness distribution on the pressure side with the one from a boundary layer calculation using the experimental pressure distribution (Bräunling et al., 1988). All the models predict a large growth and then a decay of the momentum thickness on the pressure side, but they differ io the location and the magnitude of the peak of θ.

Figure 9a compares the intermittency functions f_t for the transitional two-layer and k-ω calculations. The two models predict a laminar boundary layer (i.e. f_t is small) until the shock at x/Cax≅0.8-0.85, where f_t quickly reaches unity which indicates a turbulent boundary layer, as suggested by the experiments. In the TLK calculations f_t rises faster than in the k-ω results so that just downstream the shock the turbulent viscosity predicted by the TLK model is larger than that by k-ω. The larger momentum diffusion after the shock is probably the reason why the two-layer model was not able to predict the flow separation on the suction side which was indicated by the experiments (see figure 7). In all the calculations f_t was one in the trailing edge flow region.

Figures 10,a,b compare the measured and computed total pressure profiles at the six cross sections given in figure 2. The first profile is upstream of the shock (Dss), the second, third and fourth are taken downstream of the shock (Css, Bss, Ass), and the last two on the pressure side (Bds, Ads). The experiments show that the total pressure profile on the suction side has an inflection point after the shock which is caused by strong pressure recovery and entropy increase. This inflection gradually moves away from the wall in sections Css, Bss, and Ass. Figure 10a shows that fully turbulent calculations give unrealistic results especially on the suction side where the boundary layer thickness is largely overestimated. This overestimation is reduced, but still present, downstream of the shock because the

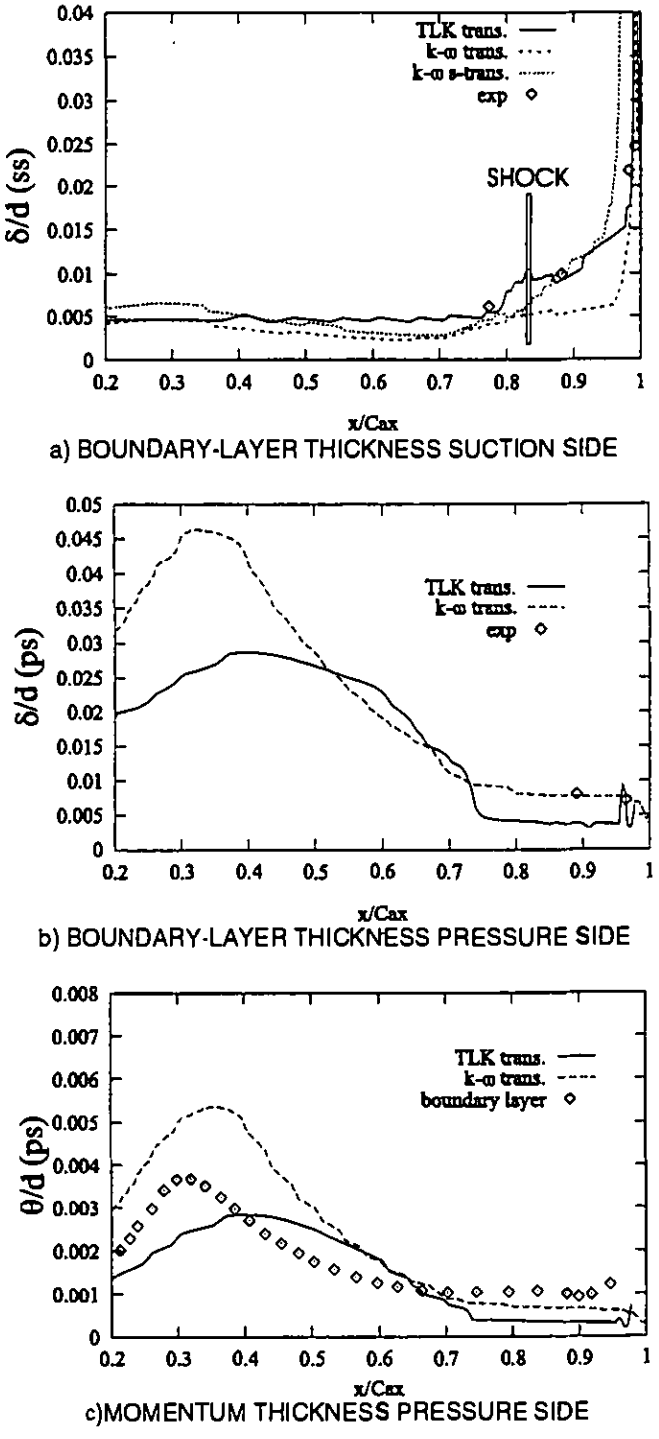

FIGURE 8. BOUNDARY-LAYER AND MOMENTUM THICKNESS

boundary layer is turbulent. Switching on the transition model improves significantly the boundary layer predictions. The transitional TLK model (Fig. 10a) can be seen to reproduce the experimental total pressure profiles better than the transitional k-ω (see figure 10b), especially in the critical region downstream of the shock where the

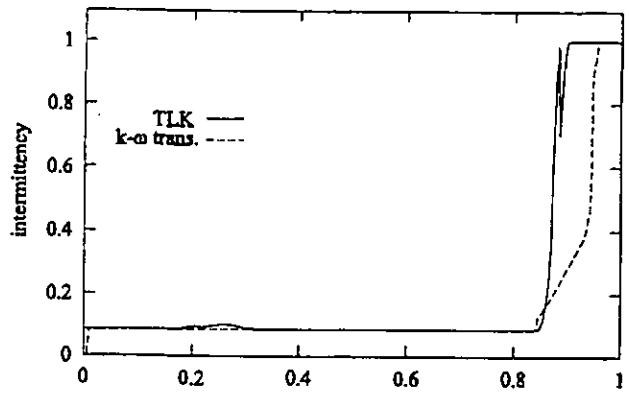

a) SUCTION SIDE

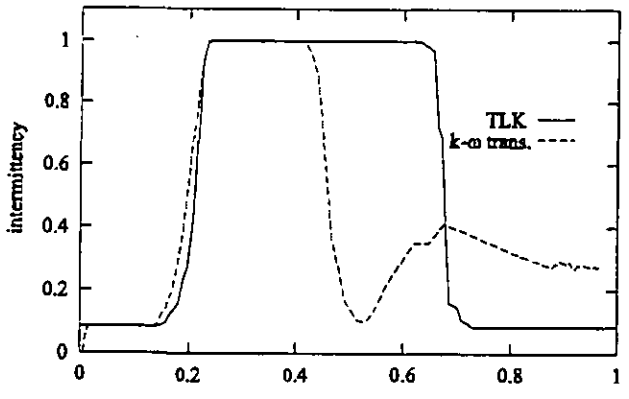

b) PRESSURE SIDE

FIGURE 9. INTERMITTENCY FUNCTION

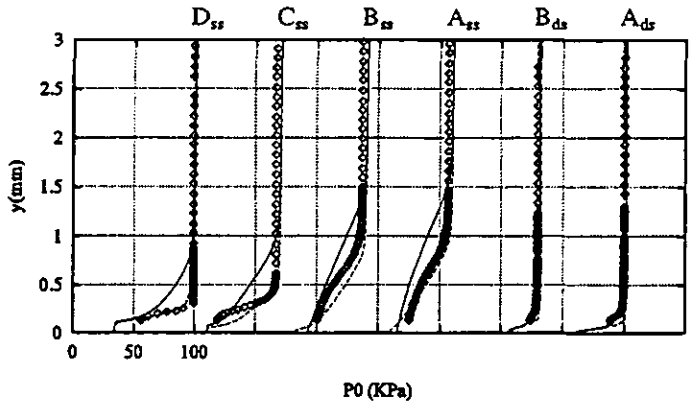

a) symbols are experiments, solid line is TLK without transition model, dash line is TLK with transition model

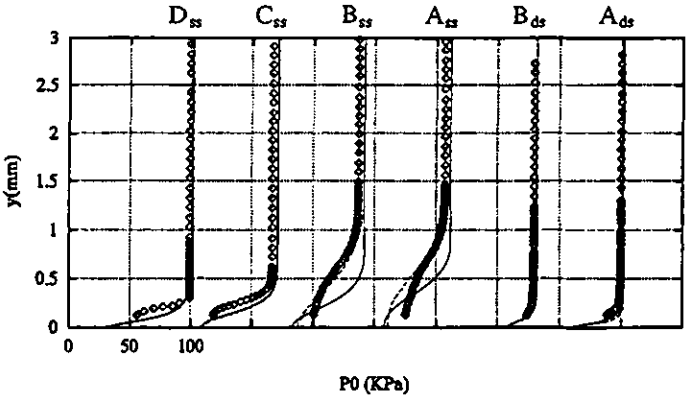

b) symbols are experiments, solid line is K-ω with attached-flow transition model, dash line is K-ω with separated-flow transition model

FIGURE 10. TOTAL PRESSURE PROFILES IN THE BLADE VANE.

experimental profiles show an inflection point which is misplaced by the latter model. In figure 10,b the s-transition model seems to perform quite well, especially across the shock. In fact this model detects a laminar separation bubble due to the shock-boundary layer interaction. Transition starts close to the end of the separation bubble, whereas the models based on the Abu-Ghannam and Shaw correlation starts transition immediately after the shock (Michelassi, 1996).

Figures 11,a,b,c report respectively the measured and computed distribution of Mach number, exit flow angle, and total pressure at a section located 1.46xCax downstream of the leading edge. The plots show only the profiles computed by the transitional TLK and k-ω models, since the fully turbulent calculations gave very similar results at this section. The Mach number profiles (figure 11a) show that the k-ω model reproduces somewhat better the peak than the TLK model. The computed up/down behavior of the profiles in the wake is more pronounced than the experimentally observed one. The predicted exit flow angle in figure 11,b shows a quite good agreement with the experiments over the full pitch range. The total pressure profiles given in figure 11,c clearly indicate a lack of wake mixing in the computations. The measured wake is considerably wider than the computed one and the minimum total pressure is larger. It should be added that the measured and computed total pressure integrals at this section are almost identical.

The experiments (Kost, 1994, Kost and Gieß, 1995) indicate that vortex shedding occurs downstream of the trailing edge. Flow visualization does not indicate this shedding in the case considered here, but the exit flow angle in the wake fluctuates between two values, as shown in figure 12 for y/t=0.243 where the exit flow angle probability density function is plotted against the pitchwise coordinate.

The same figure shows that this fluctuation is absent outside of the wake for y/t=0.794. The shedding is known to produce large mixing. This would explain the difference between the measured and calculated total pressure distribution since the steady nature of the calculations did not allow this feature to be captured, although the two counter rotating trailing edge vortices were predicted by all the models. Moreover, two-equation models are known to model incorrectly the recovery region past separations (like in the backward facing step flow): the velocity was found to recover to the boundary layer profile much slower than in experiments.

Finally, table 1 compares the computed and measured overall flow parameters. The inlet total pressure is flat, so is the inlet Mach number. The exit values, computed and measured at 1.46xCax, are mass

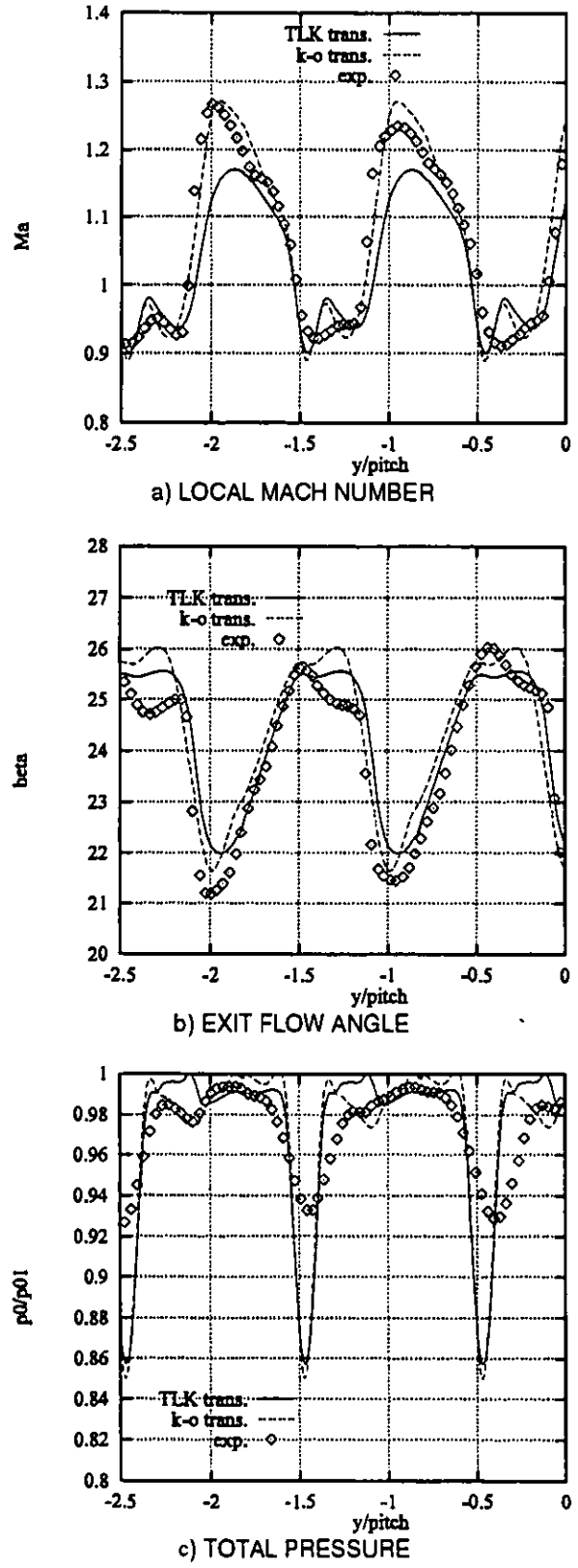

FIGURE 11. WAKE PROFILES AT X=1.46×Cax

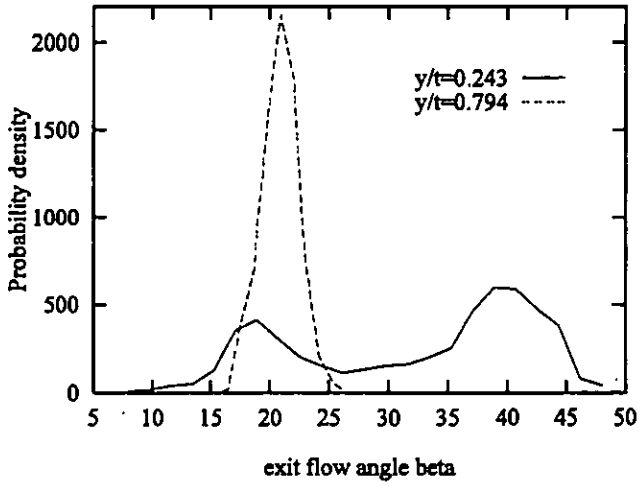

FIGURE 12. MEASURED EXIT FLOW ANGLE PROBABILITY DENSITY FUNCTION

averaged. The turbulent boundary layer calculations are shown to overestimate the total pressure losses ζ. The introduction of the transition model decreases ζ for both the TLK and k-ω models which slightly underestimates ζ. The underestimation might be caused by the extra losses in the experiments caused by the trailing edge vortex shedding. Observe that the separated flow transition model underestimates the losses because it assumes a laminar pressure side boundary layer. Inlet and outlet Mach numbers predicted with the transition models are in good agreement with experiments. The exit flow angle is overestimated 0.5-0.8-deg regardless of the transition model.

TABLE 1. Inlet and Outlet flow parameters

	M_{in}	M_{out}	β_{out} -deg	ζ (%)
exp.	0.399	1.065	23.8	3.6
k-ε wall func.	0.3869	1.033	24.2	6.63
TLK	0.3874	1.030	24.3	6.97
TLK trans.	0.390	1.045	24.24	3.16
k-ω	0.386	1.063	24.71	4.43
k-ω trans.	0.389	1.073	24.49	3.21
k-ω s-trans.	0.390	1.074	24.50	2.68

CONCLUSIONS

The detailed set of measurements allowed different turbulence and transition models to be tested in a cascade flow with shock-boundary layer interaction. The two-layer approach and the k-ω model include similar transition models which are based on the Abu-Ghannam and Shaw correlation for the onset of transition. Both models predict transition where the shock impinges on the suction side. The experiments confirm that transition occurs immediately downstream of the shock, which also induces a small flow separation that was obtained only by using the k-ω model. The size of the backflow region was rather limited and produced negligible effects on the overall flow

pattern. The empirical correlations for the onset of transition were found adequate for this test case. A separated flow transition model was also implemented in the k-ω model and gave good results. The calculations proved that turbulence and transition models are compulsory for the proper prediction of the overall flow pattern. The current set of measurements and computations indicated that also the blade load can be affected by the nature of the boundary layer. However the spreading of momentum in the wake is underpredicted due to insufficient mixing. This is due to the problems two-equation models have in the recovery region and to the steady nature of the calculations which do not allow the trailing- edge vortex shedding to be captured. The TLK and k-ω models gave very similar results because of the overwhelming importance of the transition model, whicb was the same for the two formulations.

ACKNOWLEDGMENTS

The reported experimental investigations and calculations were supported by the German Ministry of Education, Science, Research and Technology under contract no. 0326800 F and no. 0326801 G respectively within the framework of the national AG-TURBO program. The authors gratefully acknowledge this support. The authors also wish to express their gratitude to W. Bräunling who took the oil flow pictures.

REFERENCES

Abu-Ghannam, B.J., Shaw, R., 1980, "Natural Transition of Boundary Layers - The effects of Turbulence, Pressure Gradient, and Flow History", Journal of Mechanical Engineering Science, Vol.22, No.5, pp.213-228.

Amecke, J., Safarík, P., 1995, "Data Reduction of Wake Flow Measurements with Injection of an Other Gas", DLR-FB 95-32, DLR, Köln, Germany.

Bräunling, W., Quast, A., Dietrichs, H.-J., 1988, "Detection of Separation Bubbles by Infrared Images in Transonic Turbine Cascades", ASME paper 88-gt-33.

Cho, N.-H., Liu, X., Rodi, W., Shönung, B., 1993, "Calculation of Wake-Induced Unsteady Flow in a Turbine Cascade", ASME Journal of Turbomachinery, October, Vol.115, pp. 675-686.

Gieβ, P.-A., 1994, "Grenzschichtmessungen auf der Schaufeloberfläche bei transsonischer und inkompressibler Durcbströmung ebener Turbinengitter", Report IB 223 - 96 A 08, Göttingen, Germany.

Heinemann, H.-J. 1983, "The Test Facility for Rectilinear Cascades (EGG) of the DFVLR", IB 222 - 83 A 14, DFVLR, Göttingen, Germany.

Kato, M., Launder, B.E., 1993, "The Modelling of Turbulent Flow around Stationary and Vibrating Square Cylinders", Proceedings Ninth Symposium of "Turbulent Shear Flows", Kyoto, Japan, August 16-18.

Kost, F., 1993, "Längswirbelentstehung in einem Turbinenlaufrad mit konischen Seitenwänden", DLR-FB 93-13, DLR, Köln, Germany.

Kost, F., 1994, "Messungen des Geschwindigkeitsfeldes mit dem L2F-Velocimeter bei transsonischer und inkompressibler Durchströmung ebener Turbinengitter", Report IB 223-96 A 09, DLR, Göttingen, Germany.

Kost, F., Gieβ, P.-A., 1995, "Incompressible and Transonic Turbine Wake Flow Influenced by Vortex shedding". VDI Berichte NR. 1186, pp. 63-77.

Kwon, O.K., Pletcher, R.H., 1982, "Prediction of subsonic separation bubbles on airfoils by viscous-inviscid interaction". Second Symposium on Numerical and Physical Aspects of Aerodynamic Flows, Iowa State University, Ames, Iowa, USA.

Lakshminarayana B., 1991, "An Assessment of Computational Fluid Dynamic Techniques in the Analysis and Design of Turbomachinery - The 1990 Freeman Scholar Lecture", ASME J. of Fluids Eng., Vol. 113, pp. 315-352.

Mayle, R.E., 1991, "The Role of Laminar-Turbulent Transition in Gas Turbine Engines", ASME Journal of Turbomachinery, vol. I13, October, pp. 509-537.

Michelassi, V., 1994, "A pressure correction algorithm for all speed flows", Report No.718, Institute for Hydromechanik, University of Karlsruhe, Germany.

Michelassi, V., 1996, "Turbulence and Transition Modelling in Transonic Turbine Flows", Report No.728, Institute for Hydromechanik, University of Karlsruhe, Germany.

Michelassi, V., Martelli, F., (1993), "3-D Implicit Navier-Stokes Solver for Internal Turbulent Compressible Flows", Journal de Phys. III, France 3, pp. 223-235.

Michelassi, V., Papanicolaou, E., Theodoridis, G., 1995a, "A Comparison of Time Marching and Pressure Correction Algorithms for Transonic Turbine Blades", 1995 International Mechanics Engineering Congress and Exposition, November 12-17, San Francisco, California, USA.

Michelassi, V., Theodoridis, G., Papanicolaou, E., 1995b, "Low Speed Turbine Computation by Pressure Correction and Time Marching Methods", 1995 International Mechanics Engineering Congress and Exposition, November 12-17, San Francisco, California, USA.

Norris, L.H., Reynolds, W.C., 1975, "Turbulent Channel Flow with Moving Wavy Boundary", Rept. No. FM-10, Stanford University, Dept. of Mech. Eng..

Papanicolaou, E., 1996, "Computation of Separated Flow Transition Using a Two-layer Model of Turbulence", Report No.773, Institute for Hydromechanik, University of Karlsruhe, Germany.

Rodi, W., Bonnin, J.-C., Buchal, T. (Ed.), 1995, Proceedings of ERCOFTAC Workshop on "Data Bases and Testing of Calculation Methods for Turbulent Flows", University of Karlsruhe, Karlsruhe, Germany, April 3-7.

Rodi, W., Mansour, N.N., Michelassi, V., "One-Equation Near-Wall Modelling with the Aid of Direct Simulation Data", ASME Journal of Fluids Engineering, vol.115, June 1993, pp.196-205.

Rodi, W., Shönung, B., 1987, "Interaktives-Inverses Grenzschichtverfahren zur Berechnung von lokalen Ablöseblasen an Turbinenschaufeln", Z. Flugwiss. Weltraumforsch. 11, pp. 271-280.

Savill, A.M., 1993, "Further Progress in the Turbulence Modelling of By-Pass Transition", Proceedings 2-nd International Symposium on Engineering Turbulence Modelling and Measurements", May 31-June 2, Florence, Italy.

Schodl, R. A, 1980, "Laser-Two-Focus (L2F) Velocimeter for Automatic Flow Vector Measurements in Rotating Components of Turbomachines", J. Fluid Eng., vol. 102, pp. 412-419.

Wilcox, D.C., 1988, "Reassessment of the Scale-Determining Equation for Advanced Turbulence Models", AIAA Journal, Vol. 26, No.1I, pp. 1299-1310.

Zhu, J., 1992, "An Introduction and Guide to the Computer Program FAST-3D", Report No. 691, Institute for Hydromechanik, University of Karlsruhe.